JOURNAL OF Applied Polymer SCIENCE

Fabrication and Characterization of Multiwalled Carbon Nanotubes/Silicone Rubber Composites

Nadeem Iqbal,[1] Mohammad Bilal Khan,[2] Sadia Sagar,[1] Asghari Maqsood[1]
[1]School of Chemical & Materials Engineering (SCME), NUST, Islamabad, Pakistan
[2]Centre for Energy Systems (CES), NUST, Islamabad, Pakistan
Correspondence to: N. Iqbal (E-mail: nadeeem.iqbal313@hotmail.com)

ABSTRACT: To enhance the ablation performance and mechanical strength of silicone rubber (SR), pristine multiwalled carbon nanotubes (MWNTs) were dispersed in the polymer matrix using dispersion kneader and two roller mixing mill. Electrical resistivity (100–300°C) was reduced with increasing filler concentration in the host matrix due to the presence and even dispersion of the nanofiller in the rubber matrix. The SR nanocomposite (1 wt % filler contents) has 28% better thermal stability and 100% improvement in the ultimate tensile strength is achieved as compared with the pristine polymer matrix counterpart. Oxy-acetylene torch was used to evaluate the ablation rates, % char yield, and backface temperature evolution at the back facet of nanoablators during the flame exposure for a specific duration. Ablation performance of the fabricated ablative nanocomposites was enhanced with increasing nanotubes concentration in the polymer matrix. Thermal stability and heat quenching ability of the SR nanocomposites were gradually augmented with increasing filler loadings in the host matrix. Porous silica char, polymer pyrolysis, char composition, and uniform dispersion of MWNTs in the rubber matrix were also analyzed using scanning electron microscopy and energy dispersive spectroscopy. © 2012 Wiley Periodicals, Inc. J. Appl. Polym. Sci. 000: 000–000, 2012

KEYWORDS: multiwalled carbon nanotubes; silicone rubber; ablative nanocomposites; mechanical properties; Thermal stability

Received 1 June 2012; accepted 27 July 2012; published online
DOI: 10.1002/app.38410

INTRODUCTION

Ablation is a mass reduction process of a material due to the action of heat fluxes and thermomechanical loads due to the gas flows and shear stresses generated during the reentry of space vehicles and intercontinental ballistic missiles (ICBM) flight.[1,2] Elastomeric ablative composite materials are frequently used as heat shielding materials. Phenolic resins, elastomers [Nitrile butadiene rubber, Styrene butadiene rubber, Ethylene propylene diene monomer rubber, Silicone rubber (SR) etc.], carbon–carbon and ceramic (ZrC, Titanium diboride, Alumina etc.) matrices are used to fabricate ablative composites. Nanofillers [silica, carbon, carbon nanotubes (CNTs), carbon fiber, alumina, zirconia, etc.] and woven/chopped fibers (glass, ceramic, carbon etc.) have used as reinforcements in these polymer matrices.[3–8] Polymeric ablative composites limit the heat conduction in hyperthermal environment encountered by reentry vehicles/ICBM, through their charring, surface reradiational, transpirational cooling, polymer pyrolysis, char reinforcement reactions, and vaporization effects.[9–14] SR has remarkable performances in low (−200°C) as well as high (500°C) temperature environments due to high thermal stability, low density, high heat capacity, and low thermal conductivity. CNTs have tremendous mechanical, electrical, magnetic and thermal properties and due to their spectacular character, they are used in aerospace, electronic, electrical, and sports industries. Nanosilica, nanoclay, SiC-coated CNTs, and carbon fibers have been incorporated in the SR/paste to examine the thermal, mechanical and ablation characteristics of the fabricated composites, previously. The before mentioned fillers have effectively influenced the thermal/mechanical properties and ablation resistance of the rubber matrix.[15–19]

In this work, four diverse loadings of pristine multiwalled carbon nanotubes (MWNTs) are incorporated in the SR matrix using dispersion kneader and two roller mixing mill to disperse the nanotubes evenly in the polymer matrix. Ablation, thermal, and mechanical properties are examined of the fabricated nanocomposites.

High temperature ablation testing in parallel flow (PF) and head on impingement (HOI) mode of oxy–acetylene flame to determine the *in-situ* backface temperature evolution, linear/radial/mass ablation resistance, % char yield of the MWNT/SR composite specimens, and the analysis of the effect of nanotubes

Applied Polymer SCIENCE

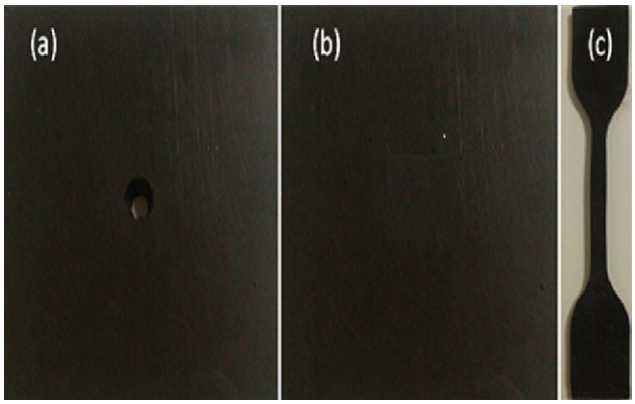

Figure 1. Photographs of the fabricated 1 wt % MWNT/rubber composites for PF (a) and HOI (b) configurations and tensile testing specimen (c). [Color figure can be viewed in the online issue, which is available at wileyonlinelibrary.com.]

concentration on aforementioned properties of the polymer matrix are the novel characteristics of this research.

EXPERIMENTAL

Materials

MWNTs (fabricated through CVD method with Fe catalyst, Purity > 95%, diameter 20–30 nm, and length 50–70 μm, average aspect ratio 2400 : 1) were purchased from Nanoport, China and they were used as received. SR (SN-7280) was purchased from Jiangyin Huaqiang Rubbers & Plastics, China. Dibenzoyl peroxide was purchased from Jiangsu Yuanyang Pharmaceutical, China.

Fabrication of MWNTs/SR Nanocomposites

Uniform dispersion of MWNTs in polymeric matrixes is a challenging task.[20,21] This goal is achieved using dispersion kneader and two roller mixing mill for the uniform dispersion of MWNTs in the SR matrix. The dispersion kneader was kept at 140°C for 40 minutes during the filler mixing in the rubber matrix. Then addition of crosslinker and the post mixing of nanotubes were carried out on two roller mixing mill at 70°C and 40 rpm roller's speed for 20 min. Various types of composite samples were fabricated at different MWNTs loading levels on two roller mixing mill which imparts leading, mixing, and elongation flow during the passage of material through the twin roll nip. The procedure is a customary practice in the rubber industry and ensured the even distribution of filler in the host matrix. Two types of ablative composite specimens according to ASTM E285-08 were fabricated on the hot isostatic press at 140°C, and 1500 psi for 50 min, that were 100 × 100 × 10 mm^3 (P ablator) and 100 × 100 × 10 mm^3 with 10 mm diameter cavity in the center (R ablator). Four specimens for each composition were amassed in each turn according to the above processing conditions as shown in Figure 1(a, b). Similar process was adopted to fabricate the tensile testing samples according to ASTM D412-98 A and for each turn six samples were collected. P ablators were used to investigate the linear ablation resistance and backface temperature evolution during the ablation testing in HOI mode of oxy–acetylene (O–A) torch flame.

Table I. Composition Scheme for the Ablative Composites

Sample ID	S10	S11	S12	S13	S14
Carbon nanotubes (wt %)	0	0.1	0.3	0.5	1.0
Silicone rubber (100 wt %) and DBP (0.5 wt %)					

DBP: dibenzoyl peroxide.

Radial/mass ablation rates and % char yield were measured for R ablated specimens, i.e., ablated in PF of O–A flame trough the 10 mm cavity. HOI is meant to simulate the direct impingement of shock waves or flame fronts on the aerodynamic/included surfaces in reentry or propulsion modules. While PF configuration simulates the shear effects generated on the bounding walls of flow such as encountered at the aft end and nozzle throat of propulsion modules. The photographs of P/R ablators and tensile testing sample are portrayed in Figure 1.

Composition of P&R Ablators

Table I elucidates the five different formulations of rubber composites with 0–1 wt % progressive incorporations of MWNTs in the rubber matrix.

Ablation Testing

Backface Temperature Recording. Ablation testing of P & R ablators was carried out using ASTM 285-08 in HOI and PF modes of O–A flame.[22] Experimental setup for the anti-ablation study of ablative nanocomposites is demonstrated in Figure 2. O–A torch was used as a high temperature source (Flame temperature ≈ 3000°C with heat flux of 8 × 10^6 W/m^2 measured with pyrometer IRAH35 U, Japan), i.e., exposed on the central front facet of the P ablator and the flame passed through the 10 mm cavity in case of R ablator. The flow rate of both Oxygen and acetylene gases was 0.35 m^3/h and their pressures were 50 psi and 23 psi, respectively during the ablation testing. The torch was kept at 10 mm far from the P ablator surface. Three thermocouples (K type) having temperature sensing range −200°C to 1350°C, were used at the backface central region of the P ablator. These thermocouples linked with the data logger

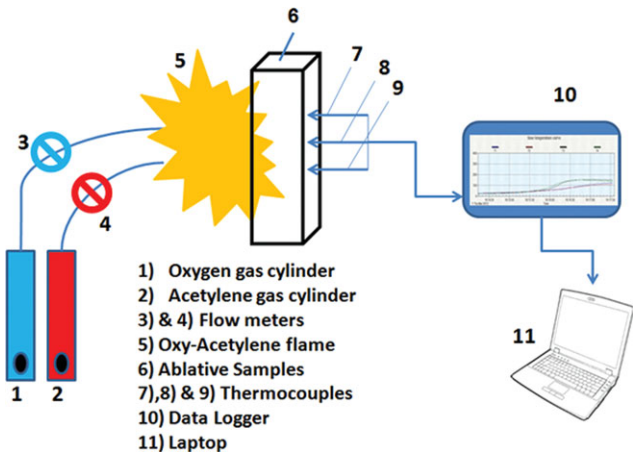

Figure 2. Schematic illustration of the experimental setup for ablation testing. [Color figure can be viewed in the online issue, which is available at wileyonlinelibrary.com.]

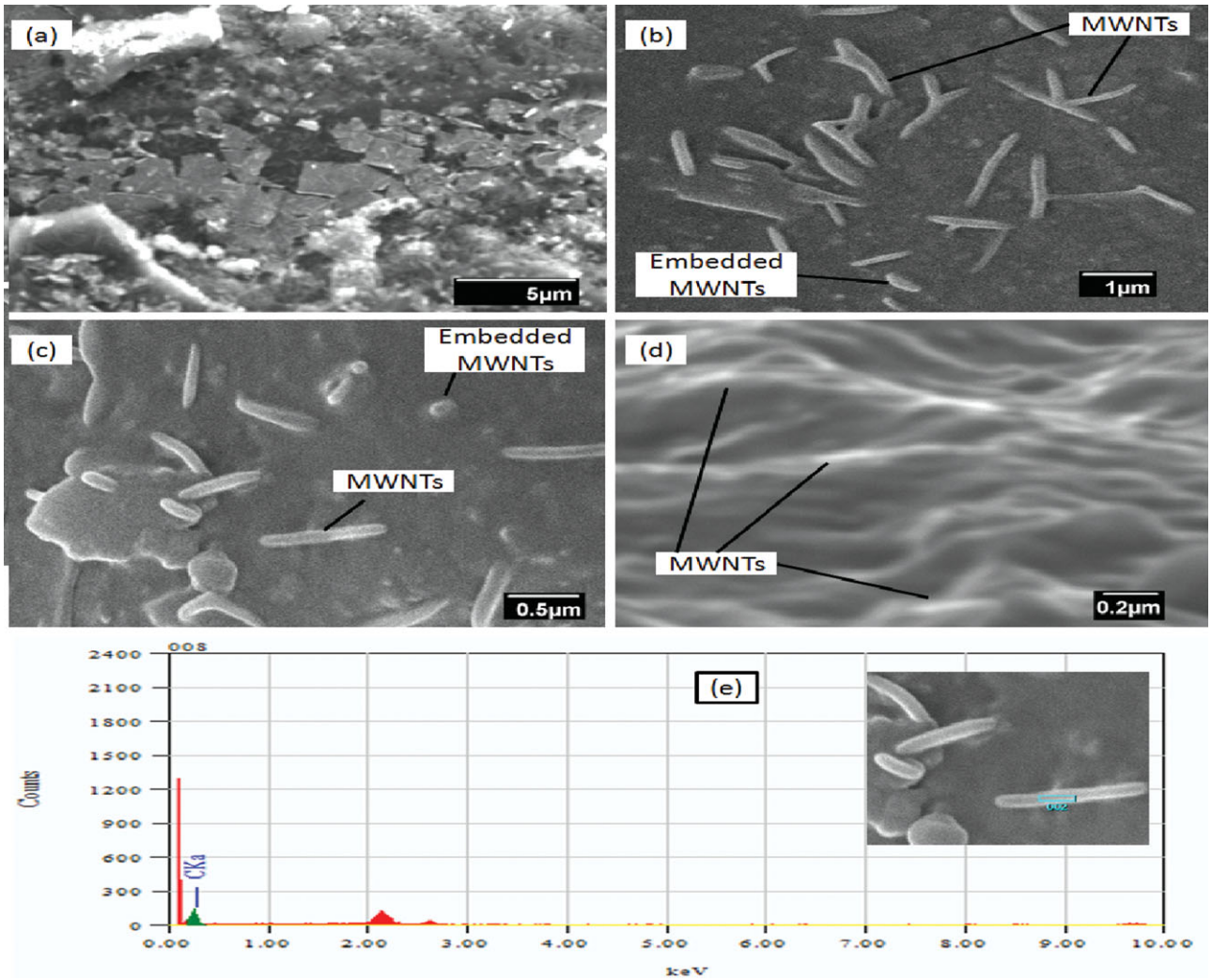

Figure 3. (a, b, c, d, e) SEM micrographs at diverse magnifications, which show the dispersion of MWNTs (1 wt % loading) in the SR matrix and spot elemental analysis of nanotube. [Color figure can be viewed in the online issue, which is available at wileyonlinelibrary.com.]

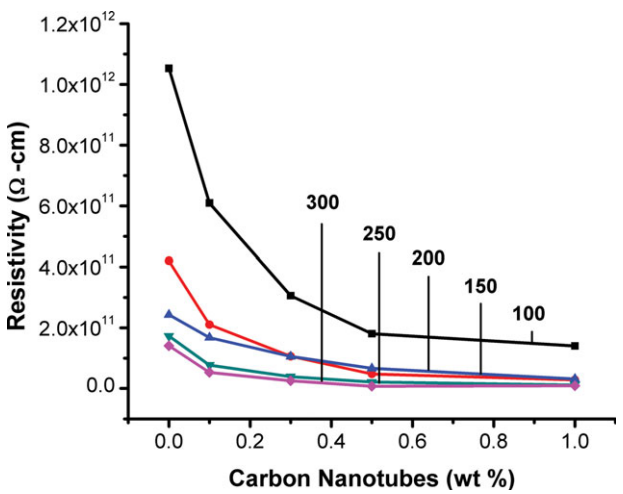

Figure 4. DC resistivity decline with various MWNTs loadings in the rubber matrix at different temperatures. [Color figure can be viewed in the online issue, which is available at wileyonlinelibrary.com.]

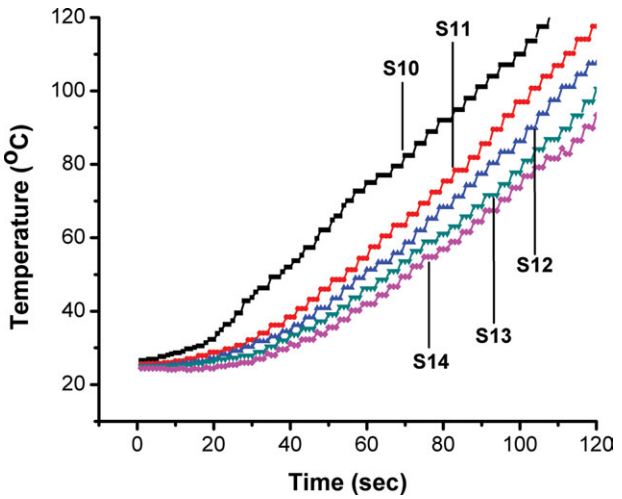

Figure 5. Effect of MWNTs contents on the temperature evolution during the ablation testing of ablative nanocomposites. [Color figure can be viewed in the online issue, which is available at wileyonlinelibrary.com.]

Applied Polymer SCIENCE

TECPEL 319, i.e., also connected to the laptop with RS-232 data cable. Time–temperature online contours for a specific duration were established on the laptop screen during the O–A torch exposure on the P ablator's facet. Porous char morphology, silica formation, char reinforcement reaction and char composition of burnt ablators were analyzed using scanning electron microscopy (SEM, JSM 6490 A, Jeol, Japan) coupled with energy dispersive x-ray spectroscopy (EDS). The composite specimens were fractured in the liquid nitrogen and coated with gold (30 nm) to make them conductive for SEM analysis and their cross-sectional area was analyzed to observe the MWNTs dispersion and other features of the ablative nanocomposites.

Ablation Rates. Linear/radial/mass ablation rates and % char yield for P & R ablators were measured according to the following formulae.

$$\text{Linear ablation rate for P ablator} = v_{pl} = (T_1 - T_2)/t \quad (1)$$

$$\text{Mass ablation rate for P ablator} = v_{\text{pm}} = (M_1 - M_2)/t \quad (2)$$

$$\text{Radial ablation rate for R ablator} = v_{\text{rl}} = (D_1 - D_2)/t \quad (3)$$

$$\text{Mass ablation rate for R ablator} = v_{\text{pm}} = (M_1' - M_2')/t \quad (4)$$

$$\%\ \text{char yield for P ablator} = \text{Y}_\text{p} = (\text{M}_1 - \text{M}_2) \times 100/\text{M}_1 \quad (5)$$

$$\%\ \text{char yield for R ablator} = \text{Y}_\text{r} = (\text{M}_1' - \text{M}_2') \times 100/\text{M}_1' \quad (6)$$

where T_1, M_1, and T_2, M_2 are the thickness and mass of the P ablator before and after ablation testing, respectively. D_1, M'_1, and D_2, M'_2 are the diameter and mass of the R ablator before and after O–A flame exposure, respectively and t is the ablation testing duration.

Thermal Stability

Perkin Elmer diamond TG/DTA was used to analyze the thermal degradation and endothermic/exothermic response of the SR ablative composites within the temperature range 25°C to 850°C.

Mechanical Properties

Mechanical properties of the ablative composite specimens were evaluated using universal tensile testing machine (AG-20KNXD Plus, Shimadzu) according to the ASTM standard D412-98 A.

Electrical Resistivity Measurements

The DC resistivities of the ablative composite specimens were conducted on the source meter (Keithley) to observe the influence of MWNTs loadings on the electric properties of SR matrix at diverse temperatures, i.e., 100°C, 150°C, 200°C, 250°C, and 300°C by placing the sample holder in a heating source.

RESULTS AND DISCUSSION

The dispersion of MWNTs in the SR matrix was achieved using a dispersion kneader followed by their post mixing on a two roller mixing mill. The dispersion of embedded MWNTs in the rubber matrix can be scrutinized in the SEM micrographs at four different magnifications as elucidated in Figure 3(a–d). Spot elemental analysis of MWNTs implanted in the host matrix is depicted in Figure 3(e) that showed the presence of 100% carbon in the nanotube.

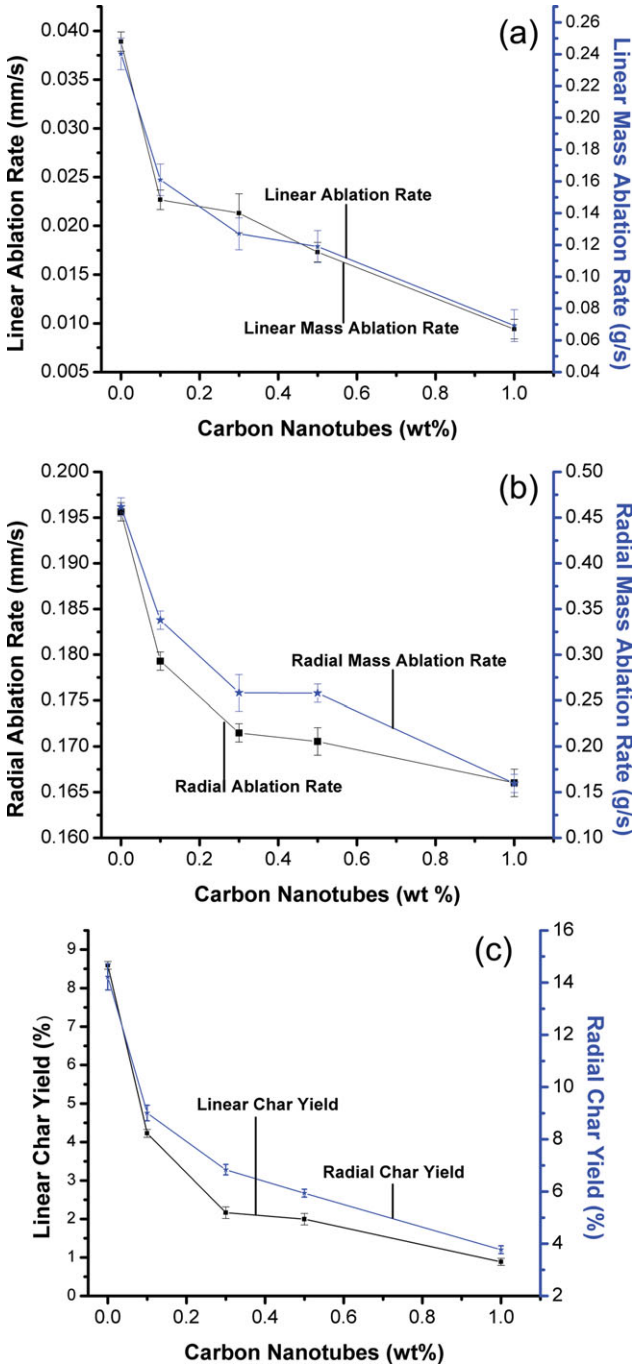

Figure 6. Improvement in linear/mass ablation resistance (a) and radial/mass ablation resistance (b) with increasing CNTs loading in the SR matrix. (c) Reduction of % char yield with increasing CNTs loading in the SR matrix. [Color figure can be viewed in the online issue, which is available at wileyonlinelibrary.com.]

Electrical resistivity was measured for all five SR composite specimens and the influence of MWNTs loadings on the dc resistivity of SR matrix is depicted in Figure 4. Electrical resistivity is reduced with the addition of nanofiller contents in the host matrix and with increasing sample holder's temperature. At 100°C, 150°C, 200°C, 250°C, and 300°C, DC resistivity for SR

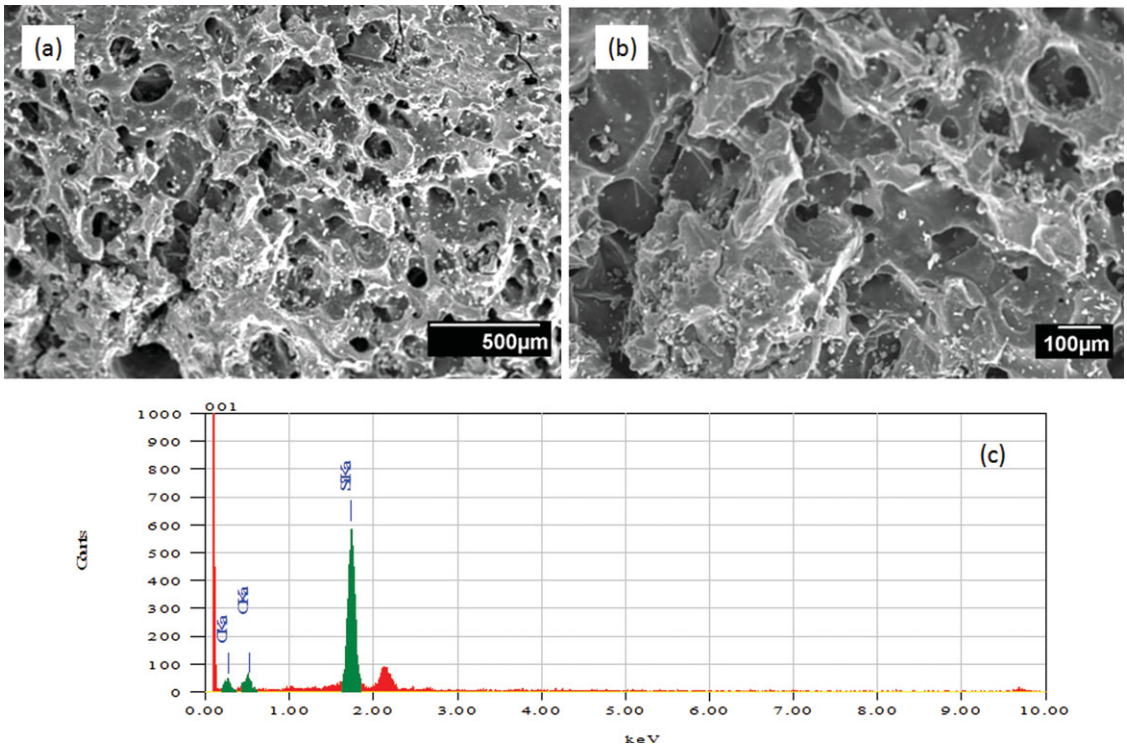

Figure 7. Scanning electron microscopy micrographs (a, b) and elemental analysis for charred ablator with 1 wt % MWNTs loading in the rubber matrix. [Color figure can be viewed in the online issue, which is available at wileyonlinelibrary.com.]

matrix was reduced 87%, 91%, 87%, 93%, and 37%, respectively with incorporating 1 wt % MWNTs in the polymer matrix. Therefore, the decline of electrical resistivity with increasing filler concentration in the elastomeric matrix was encountered due to the presence and well dispersion of MWNTs in the rubber matrix.[23–25]

The average temperature evolution rates during the 120 seconds of O–A flame exposure are (0.872, 0.766, 0.687, 0.630, and 0.575) for S10, S11, S12, S13, and S14 and this decline exhibits that the incorporation of MWNTs in the SR matrix has remarkably reduced the temperature elevation at the backface of the P ablators as illustrated in Figure 5. The reason for the minimum

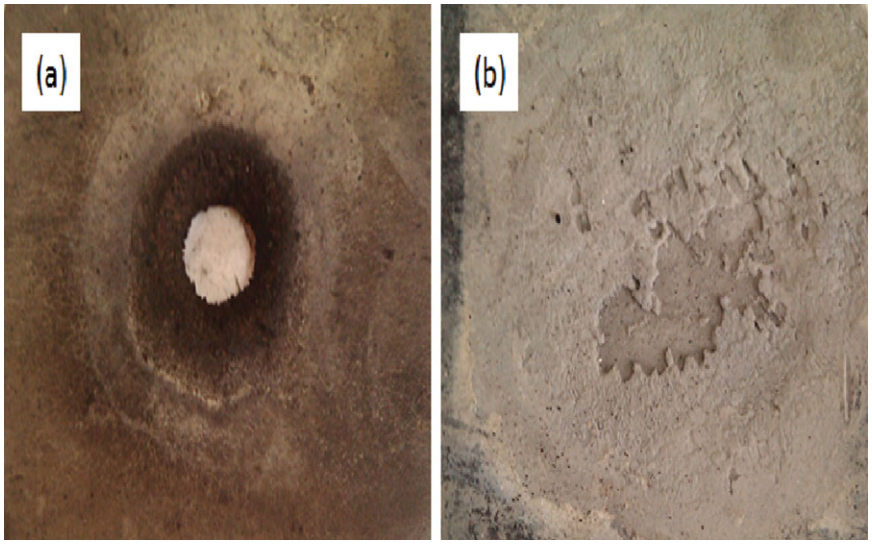

Figure 8. Photographs of the post burnt 1 wt % MWNT/rubber composite in PF mode (a) and head on collision mode (b) of oxy–acetylene flame. [Color figure can be viewed in the online issue, which is available at wileyonlinelibrary.com.]

Applied Polymer SCIENCE

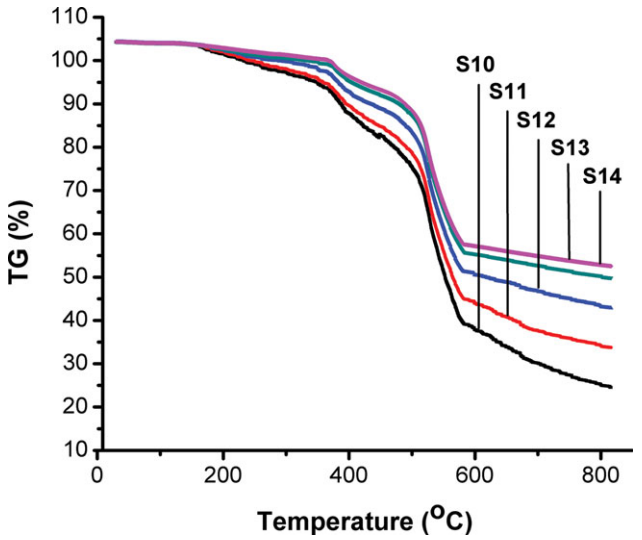

Figure 9. Thermal stability enhancement with increasing CNTs loading in the SR matrix. [Color figure can be viewed in the online issue, which is available at wileyonlinelibrary.com.]

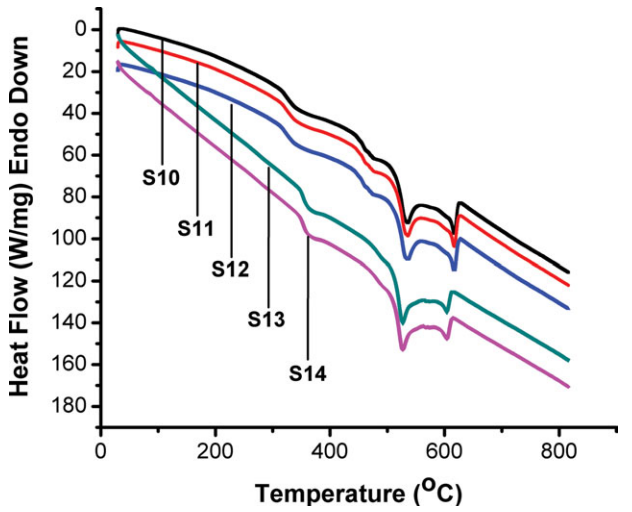

Figure 10. Heat quenching augmentation with increasing CNTs loading in the SR matrix. [Color figure can be viewed in the online issue, which is available at wileyonlinelibrary.com.]

temperature growth rate and peak temperature at the backface of P ablator (S14) is the thermal endurance and well dispersion of MWNTs in the host polymer matrix and also due to nanoscale interaction of nanotubes with the polymeric chains. During the O–A torch exposure, MWNTs constraints the thermal motion of polymer molecular chains of the SR matrix that helps to improve the thermal stability of the rubber composite.[26] SR ablators block the incoming heat flux of O–A gases through the endothermic phenomena occurred within the ablator, i.e., water and hot gases evaporation, polymer pyrolysis, surface reradiation, silica formation and melting during ablation and in addition, heat quenching by the MWNT's incorporated in the rubber matrix.

Linear/radial and mass ablation rates were evaluated for P & R ablators according to the eqs. (1)–(6).[27] Linear/mass ablation rates (v_{pl}, v_{pm}, v_{rl}, v_{rm}) are depicted in Figure 6(a, b) and the reduction in ablation rates is noticed with the wt % increase of filler contents in the SR matrix due to the high thermal stability of MWNTs.

Least linear/mass ablation rates are observed for S14 P ablator, i.e., 0.01 mm/s and 0.069 g/s, respectively due to the utmost MWNTs incorporation in the polymer matrix. The similar

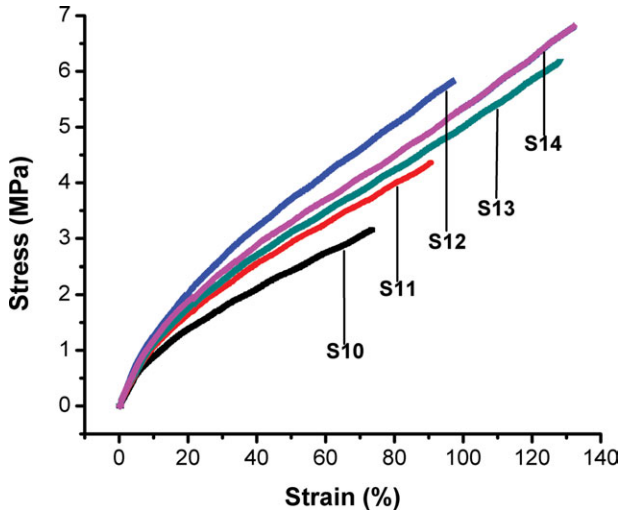

Figure 11. Tensile strength improvement with increasing CNTs loading in the SR matrix. [Color figure can be viewed in the online issue, which is available at wileyonlinelibrary.com.]

Table II. Improvement in Thermal Stability with Increasing Carbon Nanotubes Loading in the Silicone Rubber Matrix at Diverse Temperatures

Sample ID	% wt loss at 300°C	% wt loss at 500°C	% wt loss at 650°C	% wt loss at 800°C
S10	3.08	24.69	66.15	75.05
S11	2.09	21.65	59.27	65.64
S12	0.04	16.82	51.14	56.48
S13	0.02	12.75	45.79	49.89
S14	0.01	11.47	44.03	47.33

Table III. Influence of MWNTs Loadings on the Mechanical Properties of Silicone Rubber

Sample ID	Tensile strength (MPa)	Elongation at break (%)	50% Modulus (MPa)	100% Modulus (MPa)
S10	3.15	73.437	2.41	-
S11	4.34	90.449	2.90	-
S12	5.82	97.261	3.12	-
S13	6.18	128.48	3.31	5.00
S14	6.71	132.21	3.70	5.37

behavior is examined for the R ablator in case of v_{Rm} and v_{rm} but the lowest radial ablation rate is 0.166 mm/s and mass ablation rate is 0.159 g/s for S14, i.e., higher than the P ablator counterpart. It is due to the shear flow of the flame gases that were passed through the 10 mm cavity of R ablator during the ablation test. % char yield for P and R ablated samples were measured using eqs. (5) and (6), i.e., depicted in Figure 6(c) and the maximum and minimum % char yield for P and R ablators are measured as (8.590, 14.219) and (0.886 and 3.769) for S10 and S14, respectively, which shows that % char yield is also reduced with the insertion of MWNTs in the host matrix. Reduction in % char yield of an ablator indicates higher mass ablation/mechanical erosion resistance, so it can survive in hyperthermal/hypersonic environment for extended duration.

Porous silica char, silica formation, and polymer pyrolysis of the ablated composite samples at different magnifications are portrayed in Figure 7(a, b). The formation of voids during the O–A flame exposure, helps to enhance the transpiration and vaporization cooling effects happened within the ablator and this phenomenon enhances the ablation resistance and controls the backface temperature evolution during the ablation testing of ablative nanocomposites.[27] The EDS analysis in Figure 7(c) elaborates the presence of silicon, oxygen, and carbon elements in the ablated sample.

Figure 8(a, b) demonstrates the post burnt P/R ablators in PF/HOI modes of O–A flame, respectively. Apparently, adequate adhesion between the char zone and virgin material is observed after ablation testing, which is favorable for mechanical erosion resistance, i.e., a key parameter in hyperthermal and hypersonic environments encountered by an aerodynamic surface during its mission.

Thermogravimetric analysis (TGA) of the ablative composite specimens in Figure 9 elucidates the thermal degradation with temperature evolution up to 850°C. The % weight loss at 300°C, 500°C, 650°C, and 800°C during the TGA for all SR ablative composite and improved thermal stability of the polymer matrix is observed in Table II for MWNTs loaded samples compared to the pristine matrix. S14 has 28% access thermal endurance than the S10 due to the incorporation of MWNTs in the host matrix. The maximum thermal degradation is observed in the range 400–600°C for all ablators as the polymer pyrolysis of SR matrix is usually analyzed within this temperature range but MWNTs reduced this weight degradation significantly.[28]

Figure 10 elaborates the differential thermal analysis of ablative nanocomposite specimens in the temperature range 25–850°C. Although, all SR composites absorb heat but with the addition of MWNTs, endothermic nature of nanoablative specimens enhances drastically as phonons entrapped within the nanotubes as reported by Aliev et al.[29] Ablative nanocomposites S14, S13, S12, and S11 have absorbed 47%, 36%, 15%, and 5% additional amount of input heat, respectively, at 800°C than the pristine rubber matrix (S10) due to the gradual increment of CNTs in the rubber matrix. Augmentation in thermal stability and heat absorbance with increasing carbon nanotubes loading in the SR matrix has proved the efficacy of nanofiller to enhance the thermal endurance of the rubber matrix.[30]

Mechanical properties including tensile strength, elongation at break, and 50% & 100% modulus are illustrated in Figure 11 and Table III. The 1% addition of MWNTs in the SR matrix has elevated the tensile strength up to 100%, elongation at break promoted to 80%, and 50% modulus raised to 53.5% as compared with the pristine polymer. This happens due to the extraordinary mechanical properties and well dispersion of MWNTs in the host matrix.[31]

CONCLUSION

A fine dispersion of MWNTs is achieved through their pre/post mixing using dispersion kneader and two roller mixing mill, respectively. Electrical resistivity of ablative nanocomposites is reduced due to the presence of conductive MWNTs in the SR matrix. Anti-ablation and backface temperature performance of the fabricated ablators is enhanced with increasing MWNTs contents in the polymer matrix. Thermal stability and heat quenching ability of the nanocomposite specimens are elevated with the addition of MWNTs in host matrix. Augmentation in the ablation, mechanical and thermal properties with the incorporation of MWNTs in the SR matrix is noticed, that enlightened the worth of the nanofiller to fabricate elastomeric high temperature ablative nanocomposites.

ACKNOWLEDGMENTS

The authors acknowledge that this work has been completed with the cooperation of Longman Mills, Lahore and Pakistan Railway Carriage Factory, Islamabad.

REFERENCES

1. Jong, K. P.; Donghwan, Cho.; Tae, J. K.; *Carbon* **2004,** *42*, 795.
2. Wen, S. L.; *Int. J. Heat Mass Trans.* **2005,** *48*, 5504.
3. Guoxin, G.; Zhicheng, Z.; Xuefei, L.; Qingjie, M.; Yuansuo, Z.; *Polym. Bull.* **2010,** *64*, 607.
4. Maurizio, N.; Marco, M.; Debora, P.; José Maria, K.; Luigi, T.; *Compos. Part A* **2012,** *43*,174.
5. Shuguo, C.; Haiyang, Y.; Wentan, R.; Yong, Z. *Thermochim Acta* **2009,** *491*, 103.
6. Eung, S. K.; Tea, H. L.; Sung, H. S.; Jin-San, Y. *J. Appl. Polym. Sci.* **2011,** *120*, 831.
7. Changqing, H.; Jiecai, H., Xinghong, Z.; Songhe, M. *Mater. Sci. Eng. A Struct.* **2007,** *447*, 95.
8. Smrutisikha, B. *Bull. Mater. Sci.* **2010,** *33*, 27.
9. Pulci, G.; Tirillò, J.; Marra, F.; Fossati, F.; Bartuli, C.; Valente, T. *Compos. Part A* **2010,** *41*, 483.
10. Rajkumar, K.; Nivashri, K.; Ranjith, P., Chakraborty, S. K.; Thavamani, P.; Pazhanisamy, P.; Jeyanthi, P. *Chem. Tech.* **2011,** *3*, 1343.
11. Dimitrienko, Y. I. *J. Eng. Sci.* **1997,** *35*, 15.
12. Tae, J. K.; Seung J. S.; Kyunho, J.; Jong, K. P. *Carbon* **2009,** *44*, 833.
13. Khan, M. B.; Iqbal, N.; Haider, Z. *Key. Eng. Mater.* **2010,** *442*, 34.

14. Ahmad, R. B.; Mehrdad, K. *J. Hazard. Mater.* **2009,** *166*, 445.
15. Petkovic, D.; Issa, M.; Pavlovic, N. D.; Pavlovic, N.T.; Zentner, L. *Exp. Syst. Appl.* **2012,** *39*, 9477.
16. Ganesh, C. N.; Rajasekar, R.; Chapal, K. D. *J. Appl. Polym. Sci.* **2011,** *119*, 3574.
17. Zhang, C.; Kaushik, P.; Byeon, J. U.; Sang, M. H.; Jin, K. K. *J. Appl. Polym. Sci.* **2011,** *119*, 2737.
18. Zhijie, Y.; Weihua, Z.; Ting, H.; Yiwang, C.; Fan, L.; Zhentian, X.; Xiaofeng, W. *Surf. Rev. Lett.* **2011,** *18*, 33.
19. Liu, Y.; Zhang, L. Q.; Wang, W. C.; Hai-Tao, Y.; Lu, Y. L. *J. Appl. Polym. Sci.* **2012,** *123*, 2875.
20. Donald, R. P.; James, E. M. *Prog. Polym. Sci.* **2010,** *35*, 893.
21. Sung, W. L.; Young, E. P.; Kyu, S. C. *Macromol. Res*, **2010,** *18*, 766.
22. Firouzmanesh, M. R.; Azar, A. A. *J. Appl. Polym. Sci.* **2003,** *88*, 2455.
23. Tishkova, V.; Raynal, P. I.; Pascal, P.; Antoine, L.; Marion, L. F.; Philippe, D.; Emmanuel, F.; Wolfgang, B. *J. Comp. Sci. Tech.* **2011,** *71*, 1326.
24. Sophie, B.; Philippe, D.; Alain, P.; Christophe, L.; Colette, L. *Macromolecules* **2003,** *36*, 5187.
25. Eung, S. K.; Jeong, E. K.; Jea, H. S.; Jin-San, Y. *J. Appl. Polym. Sci.* **2008,** *110*, 1263.
26. Yue, G.; Ling-Xin, Z.; Li-Qun, Z.; Yong-Lai, L. *Polym. Degrad. Stab.* **2011,** *96*, 808.
27. Khan, M. B. *Adv. Mater.* **1997,** *97*, 57.
28. Wang, J. J.; Feng, L. J.; Lei, A. L.; Yan, A. J.; Wang, X. J. *J. Appl. Polym. Sci.* **2012,** *125*, 505.
29. Aliev, A. E.; Marcio, H. L.; Edward, M. S.; Baughman, R. H. *Nanotechnology*, **2010,** *21*, 035709.
30. Masarapu, C.; Henry, L. L.; Bingqing, W. *Nanotechnology*, **2005,** *16*, 1490.
31. Manuela, L. Q. A. K.; Rafaelle, B. R.; Maria, D. C. G.; Inez, V. P. Y. *Eur. Polym. J.* **2010,** *46*, 881.